

# Universality classes split by strong and weak symmetries

Jongjun M. Lee  <sup>1, 2, \*</sup> Myung-Joong Hwang  <sup>3, †</sup> and Igor Boettcher  <sup>1, 2, ‡</sup>

<sup>1</sup>Department of Physics, University of Alberta, Edmonton, Alberta T6G 2E1, Canada

<sup>2</sup>Quantum Horizons Alberta & Theoretical Physics Institute,

University of Alberta, Edmonton, Alberta T6G 2E1, Canada

<sup>3</sup>Division of Natural and Applied Sciences, Duke Kunshan University, Kunshan, Jiangsu 215300, China

(Dated: February 11, 2026)

Dissipative phase transitions are strongly shaped by the symmetries of the Liouvillian, yet the quantitative impact of weak and strong symmetries on critical behavior has remained unclear. We study a squeezed-photon model with single- and two-photon losses, realizing weak and strong symmetries in the simplest possible setting. The two symmetries exhibit identical Gaussian static fluctuations, whereas the order parameter and the asymptotic decay rate display distinct scaling behaviors. Our one-loop Keldysh analysis, together with cumulant-expansion numerics, reveals sharply different critical scaling with respect to the thermodynamic scaling parameter. This establishes that weak and strong symmetries lead to distinct dynamical universality classes despite originating from the same symmetry group in the closed system. Our results provide a clear quantitative demonstration that strong symmetries fundamentally reshape dissipative criticality.

*Introduction.*—Recent advances in cavity and circuit quantum electrodynamics have enabled access to ultra-strong and deep-strong light-matter coupling [1–4]. At the same time, dissipation can now be engineered with a high degree of control [5–8]. Together, these developments make driven-dissipative systems a practical platform for studying nonequilibrium collective phenomena. Among them, dissipative phase transitions have attracted considerable attention as they exhibit critical phenomena beyond the equilibrium paradigm [9–13]. They are marked by diverging time scales and enhanced steady-state fluctuations. Such transitions have been predicted and observed in a range of photonic [14–16], superconducting circuit [17–19], hybrid quantum [20–23], trapped ion [24–26], and cold-atom systems [27–30]. As dissipative phase transitions become experimentally accessible, a central question arises: which aspects of symmetry can affect universality in dissipative phase transitions, beyond what is expected from closed systems?

In open quantum systems, symmetries can be classified into two distinct types, weak and strong, which have no direct analogue in closed systems [31, 32]. While both types constrain the dynamics and can undergo spontaneous symmetry breaking, they can lead to qualitatively different dissipative behavior. Recent work has highlighted a novel strong-to-weak symmetry breaking and has introduced order parameters capable of diagnosing such transitions [33–38]. Related studies have further revealed novel topological orders of mixed states [39, 40], emergent hydrodynamic behavior [41], quantum error corrections [42–44], and measurement schemes [45, 46].

Despite this progress, a basic issue remains unresolved. It is still unclear whether weak and strong symmetries,

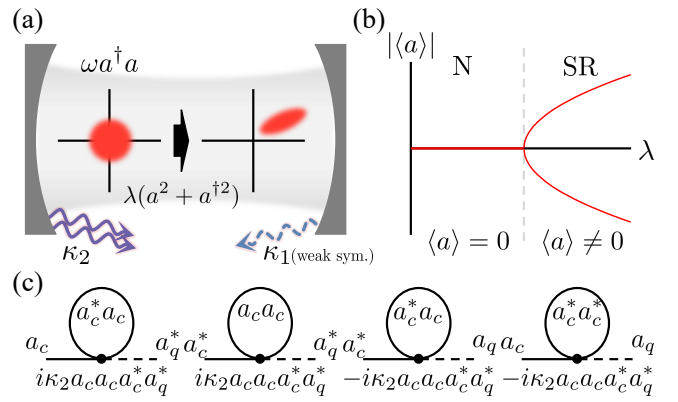


FIG. 1. Schematic illustrations of (a) the system, (b) the phase diagram as a function of the two-photon driving strength  $\lambda$ , and (c) the loop diagrams relevant to the quartic-order corrections to the retarded Green function. The single-photon loss ( $\kappa_1$ ) is present only for the weak parity symmetry. N and SR denote the normal and superradiant phases, respectively.

which are closely related at the level of the symmetry group, lead to genuinely different critical behavior in dissipative phase transitions. In particular, the extent to which the nature of symmetry controls universality in open quantum criticality has not yet been systematically established [47–50].

In this work, we focus on strong and weak parity symmetries in open quantum systems. These two symmetries share a common origin in the parity symmetry of the underlying closed system [51, 52], but differ in how the symmetry is implemented once dissipation is present [42]. We study a minimal model of a single-mode cavity photon subject to squeezing, with single- and two-photon losses providing the dissipative channels [42, 53–56]; see Fig. 1(a). By tuning the single-photon loss, we selectively realize weak or strong parity symmetry, while the squeez-

\* Contact author: jongjun@ualberta.ca

† Contact author: myungjoong.hwang@duke.edu

‡ Contact author: iboettch@ualberta.ca

ing strength controls the dissipative phase transition.

We show that weak and strong parity symmetries give rise to distinct universality classes in dissipative phase transitions. Although the two symmetries exhibit identical Gaussian fluctuations near criticality, their scaling behavior with the thermodynamic scaling parameter differs sharply beyond the Gaussian level [57–59]. Using a Keldysh path-integral analysis and an equivalent Langevin description, we obtain closed-form expressions for the critical behavior [60–63]. These analytical results are further supported by numerics based on a cumulant expansion of the equations of motion derived from the master equation [64–66].

*Model and symmetry.*—A single photonic mode is subject to two-photon driving and coupled to an environment via single- and two-photon losses. The dynamics of the density matrix  $\rho$  is governed by the Lindblad master equation,

$$\frac{\partial \rho}{\partial t} = \mathcal{L}[\rho] = -i[H, \rho] + \sum_{j=1,2} \mathcal{D}[L_j], \quad (1)$$

with the Hamiltonian

$$H = \omega a^\dagger a + \lambda(a^2 + a^{\dagger 2}). \quad (2)$$

The dissipators are defined as  $L_1 = \sqrt{\kappa_1}a$  and  $L_2 = \sqrt{\kappa_2}a^2$ , and  $\mathcal{D}[L] = 2L\rho L^\dagger - L^\dagger L\rho - \rho L^\dagger L$ . Here,  $\omega > 0$  is the photon frequency,  $\lambda \geq 0$  denotes the two-photon driving strength, and  $\kappa_1 \geq 0$  and  $\kappa_2 > 0$  are the single- and two-photon loss rates, respectively. A schematic of the system is shown in Fig. 1(a). We will use the notation  $\langle \mathcal{O} \rangle = \text{Tr}[\mathcal{O}\rho_{ss}]$  where  $\rho_{ss}$  is the steady state, i.e.,  $\mathcal{L}[\rho_{ss}] = 0$ . The two-photon driving can be induced by a parametric pump [67], while the two-photon loss can be realized by coupling the cavity mode to an auxiliary nonlinear dissipative channel [8], with residual single-photon loss arising from intrinsic decay [68].

The Lindbladian exhibits a parity symmetry whose nature depends on the presence of the single-photon loss  $\kappa_1$ . We define the parity operator  $\Pi = \exp(i\pi a^\dagger a)$ , which satisfies  $\{\Pi, L_1\} = 0$  and  $[\Pi, H] = [\Pi, L_2] = 0$  [32]. As a consequence, with finite single-photon loss ( $\kappa_1 \neq 0$ ), the Lindbladian exhibits only a weak parity symmetry,  $\mathcal{L}[\Pi\rho\Pi^\dagger] = \Pi\mathcal{L}[\rho]\Pi^\dagger$ , whereas in the absence of single-photon loss ( $\kappa_1 = 0$ ) it possesses a strong parity symmetry,  $[\mathcal{L}, \Pi] = 0$  [42]. In the presence of these symmetries, the Lindbladian decomposes into symmetry-resolved sectors, with the strong parity symmetry giving rise to decoherence-free subspaces that can protect quantum information against dissipation [69, 70]. Accordingly, in this open quantum system, the presence or absence of single-photon loss leads to a realization of either a strong or a weak parity symmetry.

*Order parameter.*—This model undergoes a dissipative phase transition at the critical driving strength  $\lambda_c =$

$\frac{1}{2}\sqrt{\omega^2 + \kappa_1^2}$  [42]. For  $\lambda < \lambda_c$ , the parity symmetry is preserved and no photon condensation occurs in the steady state,  $\langle a \rangle = 0$ , corresponding to the normal phase. For  $\lambda > \lambda_c$ , the parity symmetry is spontaneously broken, and a macroscopic photon condensate develops as an order parameter in the steady state. Near the critical point, the order-parameter amplitude obtained from mean-field theory is given by

$$|\langle a \rangle| \simeq \begin{cases} \sqrt{\frac{\lambda_c}{\kappa_1 \kappa_2}} \sqrt{\lambda - \lambda_c}, & (\kappa_1 \neq 0), \\ \frac{\omega^{1/4}}{\sqrt{2\kappa_2}} (\lambda - \lambda_c)^{1/4}, & (\kappa_1 = 0). \end{cases} \quad (3)$$

corresponding to weak and strong parity symmetries, respectively. This phase is referred to as the superradiant phase. We schematically illustrate the corresponding phase diagram in Fig. 1(b).

For the dissipative phase transition considered here, the two-photon loss rate  $\kappa_2$  plays the role of an effective thermodynamic scaling parameter. A finite  $\kappa_2$  prevents true photon condensation by inducing a finite-size crossover [10, 13], playing a role analogous to that of the inverse system size  $1/N$  in the Dicke model [52]. A sharp phase transition emerges only in the limit of vanishing  $\kappa_2$  [44, 71].

*Fluctuation and critical scaling.*—To investigate Gaussian fluctuations near the transition, we employ the Keldysh path-integral formalism. Starting from the Lindblad master equation in Eq. (1), the quadratic (Gaussian) Keldysh action takes the form

$$S^{(2)} = \frac{1}{2} \int \frac{d\nu}{2\pi} \Psi_\nu^\dagger \begin{pmatrix} 0 & [G_0^A(\nu)]^{-1} \\ [G_0^R(\nu)]^{-1} & \Sigma_0^K \end{pmatrix} \Psi_\nu, \quad (4)$$

where  $\Psi_\nu^\dagger = (\delta a_{c,\nu}, \delta a_{c,-\nu}^*, \delta a_{q,\nu}, \delta a_{q,-\nu}^*)^T$  is the Nambu-Keldysh spinor [61]. Here,  $\delta a = a - \langle a \rangle$  denotes fluctuations around the mean-field solution, and the classical and quantum components are defined as  $a_{c/q} = (a_+ \pm a_-)/\sqrt{2}$ . The retarded Green function is given by

$$[G_0^R(\nu)]^{-1} = \begin{pmatrix} \nu - \omega + i\Gamma & -2\lambda + 2i\rho \\ -2\lambda - 2i\rho & -\nu - \omega - i\Gamma \end{pmatrix}, \quad (5)$$

with the advanced Green function  $G_0^A(\nu) = G_0^R(\nu)^\dagger$ . The Keldysh self-energy is  $\Sigma_0^K = 2i\Gamma\mathcal{I}_2$ , where  $\mathcal{I}_2$  is the  $2 \times 2$  identity matrix. The effective damping rate is  $\Gamma = \kappa_1 + 4\rho$ , with  $\rho = \kappa_2|\langle a \rangle|^2$ .

The number and squeezing fluctuations,  $\delta n = \langle \delta a^\dagger \delta a \rangle$  and  $\delta m = \langle \delta a^2 \rangle$ , are obtained from the Keldysh Green function  $G_0^K(\nu) = G_0^R(\nu)\Sigma_0^K G_0^A(\nu)$  as

$$\begin{aligned} \delta n &= -\frac{i}{2} \int \frac{d\nu}{2\pi} [G_0^K(\nu)]_{22} - \frac{1}{2}, \\ \delta m &= -i \int \frac{d\nu}{2\pi} [G_0^K(\nu)]_{12}. \end{aligned} \quad (6)$$

	$\delta n$	$\text{Re}[\delta m]$	$\text{Im}[\delta m]$	$\mu$	$\Gamma_{\text{ADR}}$
W, N	$\frac{\lambda_c}{4}\epsilon^{-1}$	$-\frac{\omega}{8}\epsilon^{-1}$	$-\frac{\kappa_1}{8}\epsilon^{-1}$	$\sqrt{\frac{2}{\lambda_c}}\epsilon^{1/2}$	$\frac{4\lambda_c}{\kappa_1}\epsilon$
W, SR	$\frac{\lambda_c}{4}\epsilon^{-1}$	$-\frac{\omega}{8}\epsilon^{-1}$	$-\frac{\kappa_1}{8}\epsilon^{-1}$	$\sqrt{\frac{2}{\lambda_c}}\epsilon^{1/2}$	$\frac{4\lambda_c}{\kappa_1}\epsilon$
S, N	$\frac{\omega}{8}\epsilon^{-1}$	$-\frac{\omega}{8}\epsilon^{-1}$	0	$\frac{2}{\sqrt{\omega}}\epsilon^{1/2}$	0
S, SR	$\frac{\omega}{16}\epsilon^{-1}$	$-\frac{\omega}{16}\epsilon^{-1}$	$-\frac{\sqrt{\omega}}{8}\epsilon^{-1/2}$	$\sqrt{\frac{8}{\omega}}\epsilon^{1/2}$	$4\sqrt{\omega}\epsilon^{1/2}$

TABLE I. Summary of the scaling behavior of Gaussian fluctuations as a function of the two-photon driving strength  $\lambda$  near the critical point  $\lambda_c$ . Here,  $\epsilon \equiv |\lambda - \lambda_c|$ . W and S label the weak and strong parity symmetries, respectively, while N and SR denote the normal and superradiant phases.

Near the critical point  $\lambda = \lambda_c$ , Gaussian fluctuations diverge algebraically and exhibit power-law behavior,

$$\delta n, \text{Re}[\delta m], \text{Im}[\delta m] \propto \frac{1}{|\lambda - \lambda_c|}. \quad (7)$$

The only exception occurs for  $\text{Im}[\delta m]$  for the strong parity symmetry: it vanishes in the normal phase at the Gaussian level due to the structure of the quadratic action and instead exhibits a weaker divergence with exponent  $-1/2$  in the superradiant phase. The purity  $\mu \equiv \text{Tr}[\rho^2]$  of the steady state shows a square-root scaling on both sides of the transition, i.e.,  $\mu \propto \sqrt{|\lambda - \lambda_c|}$ . The exact coefficients of these divergences are summarized in Table I.

At the Gaussian level, both weak and strong symmetries therefore exhibit identical critical exponents for the divergence of number and squeezing fluctuations, as well as for the vanishing of the purity [61]. Although  $\text{Im}[\delta m]$  exhibits a distinct exponent in the superradiant phase of the strong parity symmetry, experimentally measured quadrature variances involve a linear combination of  $\text{Re}[\delta m]$  and  $\text{Im}[\delta m]$ , with the former providing the dominant contribution [72]. Consequently, the two symmetry classes differ only in nonuniversal coefficients and in specific correlators, rather than in the universal critical scaling. This demonstrates that Gaussian static fluctuations are insensitive to the distinction between strong and weak symmetries here, implying that symmetry-dependent critical behavior of static fluctuations must originate beyond the quadratic approximation.

*Asymptotic decay rate.*—The asymptotic decay rate  $\Gamma_{\text{ADR}}$  (ADR), defined as the smallest non-zero decay rate in the system and equivalent to the Liouvillian gap [31], controls the slowest relaxation toward the steady state. At the Gaussian level, it is determined by the poles of the retarded Green function in Eq. (5). For the weak parity symmetry ( $\kappa_1 \neq 0$ ), the ADR near the critical point exhibits linear scaling on both sides of the transition and is given by

$$\Gamma_{\text{ADR}}(\kappa_1 \neq 0) \simeq \frac{4\lambda_c}{\kappa_1} |\lambda - \lambda_c|. \quad (8)$$

In contrast, the behavior of the ADR for the strong parity symmetry ( $\kappa_1 = 0$ ) is qualitatively different. In the normal phase, the retarded Green function  $G_0^R(\nu)$  becomes purely real, implying the absence of dissipative relaxation channels [31, 32]. As a consequence, all decay rates vanish in the thermodynamic limit, and the ADR is not well defined. Physically, this reflects the emergence of an extensive manifold of stationary states with infinite lifetime [73, 74]. By contrast, in the superradiant phase, the ADR becomes finite and follows the scaling

$$\Gamma_{\text{ADR}}(\kappa_1 = 0) \simeq 4\sqrt{\omega}\sqrt{\lambda - \lambda_c}. \quad (9)$$

This square-root behavior sharply contrasts with the linear scaling found for weak parity symmetry. While this difference signals that systems with weak and strong parity symmetries belong to different universality classes, a systematic analysis of non-Gaussian fluctuations is required to fully characterize the corresponding universality classes. The above results are summarized in Table I.

*Quartic-order correction.*—We now investigate the non-Gaussian fluctuations arising from higher-order corrections at the critical point. Since there is no condensation at this point, the quartic-order action originating from the two-photon loss can be written directly in terms of the bare Keldysh fields  $a_{c/q}$  as

$$S^{(4)} = i \int dt (L_q^\dagger L_c - L_c^\dagger L_q + 2L_q^\dagger L_q), \quad (10)$$

with  $L_c = \sqrt{\kappa_2/2}(a_c^2 + a_q^2)$  and  $L_q = \sqrt{2\kappa_2}a_c a_q$ . This quartic action generates five distinct types of Keldysh vertices. We treat these interaction effects perturbatively, assuming that  $\kappa_2$  is small.

Among these vertices, those involving three classical fields and one quantum field yield corrections to the quadratic Keldysh action at the one-loop level; see Fig. 1(c). As a representative example, the retarded Green function acquires the form

$$[G^R(\nu)]^{-1} = \begin{pmatrix} \nu - \omega + i\tilde{\Gamma} & -2\lambda + 2i\tilde{\rho}^* \\ -2\lambda - 2i\tilde{\rho} & -\nu - \omega - i\tilde{\Gamma} \end{pmatrix}, \quad (11)$$

where  $\tilde{\Gamma} = \Gamma + 2\kappa_2 n$  and  $\tilde{\rho} = \rho + \kappa_2 m/2$ . Using this one-loop-corrected quadratic action, we compute both the static and dynamical fluctuations and obtain analytic expressions at the critical point as functions of  $\kappa_2$ . The exact coefficients of these results are summarized in Table II.

These results reveal that the non-Gaussian fluctuations exhibit distinct scaling behaviors with respect to  $\kappa_2$ , which plays the role of an effective thermodynamic scaling parameter, depending on whether the system possesses weak or strong parity symmetry. For instance, with the weak parity symmetry, the number fluctuation scales as  $1/\sqrt{\kappa_2}$ , whereas with the strong parity symmetry, it scales as  $1/\kappa_2^{2/3}$ . This implies that the two symme-

	$\delta n$	$\text{Re}[\delta m]$	$\text{Im}[\delta m]$	$\mu$	$\Gamma_{\text{ADR}}$
W	$\frac{\lambda_c}{\sqrt{\kappa_1 \kappa_2}}$	$-\frac{\omega}{2\sqrt{\kappa_1 \kappa_2}}$	$-\frac{1}{2}\sqrt{\frac{\kappa_1}{\kappa_2}}$	$\frac{1}{2\sqrt{\lambda_c}}(\frac{\kappa_2}{\kappa_1})^{1/4}$	$2\lambda_c\sqrt{\frac{\kappa_2}{\kappa_1}}$
S	$\frac{\omega^{2/3}}{\sqrt{6}\kappa_2^{2/3}}$	$-\frac{\omega^{2/3}}{\sqrt{6}\kappa_2^{2/3}}$	$-\frac{\omega^{1/3}}{2\kappa_2^{1/3}}$	$\sqrt{\frac{3}{2\sqrt{6}-3}}(\frac{\kappa_2}{\omega})^{1/3}$	$\frac{2\omega^{2/3}}{\sqrt{6}}\kappa_2^{1/3}$

TABLE II. Summary of the scaling behavior of non-Gaussian fluctuations as a function of the two-photon loss strength  $\kappa_2$  at the critical point  $\lambda = \lambda_c$ . W and S label the weak and strong parity symmetries, respectively.

tries belong to different universality classes, despite sharing a common symmetry operator in the corresponding closed system. This distinction constitutes the central result of this work.

*Universality classes.*—We now have analytic expressions for the scaling behaviors, both in the vicinity of the critical point as a function of the two-photon driving strength  $\lambda$  and at the critical point as a function of  $\kappa_2$ ; they are summarized in Tables I and II. Together with the scaling hypothesis, these results imply the universal scaling form of the photon number fluctuation [75, 76]

$$\delta n(\lambda, \kappa_2) = \kappa_2^{-\zeta_x} F_{w(s)}(|\lambda - \lambda_c|^{\nu_x} \kappa_2^{-\zeta_x}) \quad (12)$$

where the photon-flux exponent is  $\nu_x = 1$  for both symmetries [60], while  $\zeta_x = 1/2$  and  $2/3$  for weak and strong parity symmetries, respectively. Here,  $F_{w(s)}(x)$  is a dimensionless scaling function. The Gaussian critical behavior is recovered in the limit  $\kappa_2 \rightarrow 0$  at fixed  $\lambda \neq \lambda_c$ , which requires  $F_{w(s)}(x \rightarrow \infty) \propto x^{-1}$ . At the critical point  $\lambda = \lambda_c$  with fixed  $\kappa_2 > 0$ , the scaling function approaches a constant, consistently reproducing the non-Gaussian scaling behavior.

This scaling form already indicates that the systems with weak and strong parity symmetries belong to distinct universality classes. While the individual critical exponents  $\nu_x$  and  $\zeta_x$  depend on the observable, their ratio  $\xi_x = \nu_x/\zeta_x$  defines the coherence number and is observable-independent [24]. We obtain  $\xi_x = 2$  for weak parity symmetry and  $\xi_x = 3/2$  for strong parity symmetry. Dynamical scaling further supports this classification. The ADR yields the dynamical exponent  $\nu_t = 1, (1/2)$  with respect to  $\lambda$  and the cut-off dynamical exponent  $\zeta_t = 1/2, (1/3)$  with respect to  $\kappa_2$  for weak (strong) parity symmetry [60, 77]. The ratio  $\nu_t/\zeta_t$  again gives 2 and  $3/2$  for the weak and strong parity symmetries, in agreement with the coherence numbers extracted from the number fluctuations.

Taken together, these results identify the universality classes of the model. The system with weak parity symmetry belongs to the same universality class as the open Dicke and Rabi models with single-photon loss [24, 60], whereas the model with strong parity symmetry defines a distinct universality class.

*Numerical verification.*—Starting from the Lindblad master equation in Eq. (1), we derive the equations of

motion for the first and second moments. We have

$$\begin{aligned} \frac{d\langle a \rangle}{dt} &= -(i\omega + \kappa_1)\langle a \rangle - 2i\lambda\langle a \rangle^* - 2\kappa_2\langle a^\dagger a^2 \rangle, \\ \frac{dm}{dt} &= -2(i\omega + \kappa_1 + \kappa_2)m - 2i\lambda - 4i\lambda n \\ &\quad - 4\kappa_2\langle a^\dagger a^3 \rangle, \\ \frac{dn}{dt} &= +2i\lambda(m - m^*) - 2\kappa_1 n - 4\kappa_2\langle a^\dagger a^2 \rangle, \end{aligned} \quad (13)$$

where  $n = \langle a^\dagger a \rangle$  and  $m = \langle a^2 \rangle$ . In the steady state, the left-hand sides vanish. We truncate the hierarchy using a cumulant expansion up to second order [65, 66], which yields three coupled nonlinear equations for  $\langle a \rangle$ ,  $n$ , and  $m$ . See the Supplemental Material for the detailed derivation [78]. We note that these equations explicitly depend on  $\kappa_2$ , reflecting the inclusion of non-Gaussian effects arising from the loop corrections shown in Fig. 1(c), beyond the quadratic approximation.

We solve the resulting equations numerically. The solutions reproduce the divergence with respect to the two-photon driving strength  $\lambda$ , following the power-law behavior summarized in Table I. See the Supplemental Material for the corresponding data [78]. In Figs. 2(a)-(c), we plot the fluctuations at the critical point  $\lambda = \lambda_c$  as functions of  $\kappa_2$ . Here, the inverse two-photon loss rate plays the role of an effective thermodynamic scaling parameter. The log-log plots clearly confirm the critical ex-

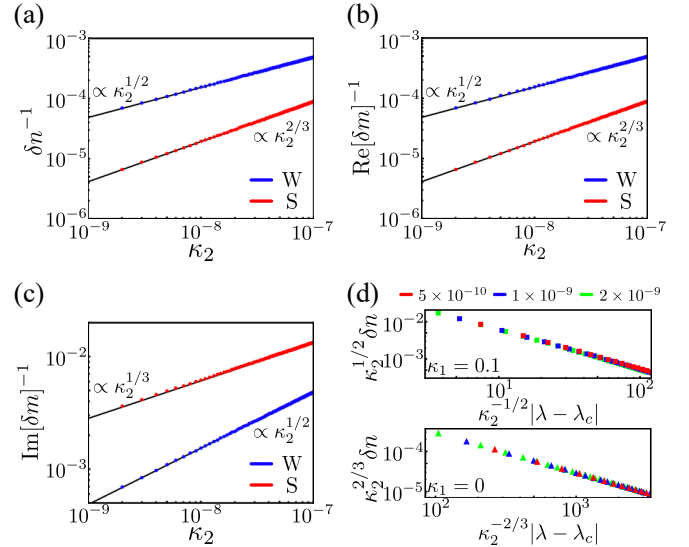


FIG. 2. Numerical results from the cumulant expansion. (a) Number fluctuation  $\delta n$ , (b)  $\text{Re}[\delta m]$ , and (c)  $\text{Im}[\delta m]$  at the critical driving strength  $\lambda_c$  as functions of the two-photon loss rate  $\kappa_2$  for weak (W) and strong (S) parity symmetries. Black lines indicate power-law fits. (d) Rescaled number fluctuation  $\kappa_2^{1/2(2/3)}\delta n$  versus  $\kappa_2^{-1/2(-2/3)}|\lambda - \lambda_c|$  in the superradiant phase for weak (strong) parity symmetries. Colors denote different values of  $\kappa_2$ . The collapse of data points onto a single curve confirms Eq. (12).

ponents analytically predicted in Table II for both weak and strong parity symmetries.

In Fig. 2(d), we present the rescaled number fluctuation  $\kappa_2^{1/2(2/3)}\delta n$  as a function of  $\kappa_2^{-1/2(2/3)}|\lambda - \lambda_c|$  for the weak(strong) parity symmetry. Note that data obtained for different values of  $\kappa_2$  collapse onto a single curve. This provides numerical evidence for a universal scaling behavior near the critical point [Eq. (12)].

*Conclusion and outlook.*—In conclusion, we have demonstrated that weak and strong parity symmetries exhibit distinct critical scaling behaviors and belong to different universality classes, despite sharing a common origin in the parity symmetry of the underlying closed system. Our results show that universality classes in dissipative phase transitions cannot be inferred solely from the symmetry group of the closed system, but instead depend crucially on how that symmetry is implemented at the level of the Lindbladian dynamics, i.e., through weak and strong symmetry realizations.

The distinction between weak and strong symmetry implementations identified here provides a concrete criterion for organizing dissipative universality classes. A pressing future direction is to examine whether this criterion extends to other symmetry settings and to spatially extended driven-dissipative systems. These predictions can be tested experimentally in cavity and circuit QED platforms where dissipative channels are controllable.

*Acknowledgements.*—We thank Min Ju Park and Canon Sun for inspiring discussions. M.-J.H. was supported by the Innovation Program for Quantum Science and Technology 2021ZD0301602. I.B. acknowledges funding from the Natural Sciences and Engineering Research Council of Canada (NSERC) Discovery Grants RGPIN-2021-02534 and DGECR2021-00043.

---

- [1] G. Günter, A. A. Anappara, J. Hees, A. Sell, G. Biasiol, L. Sorba, S. De Liberato, C. Ciuti, A. Tredicucci, A. Leitenstorfer, *et al.*, Sub-cycle switch-on of ultrastrong light-matter interaction, *Nature* **458**, 178 (2009).
- [2] T. Niemczyk, F. Deppe, H. Huebl, E. Menzel, F. Hocke, M. Schwarz, J. Garcia-Ripoll, D. Zueco, T. Hümmer, E. Solano, *et al.*, Circuit quantum electrodynamics in the ultrastrong-coupling regime, *Nature Physics* **6**, 772 (2010).
- [3] F. Yoshihara, T. Fuse, S. Ashhab, K. Kakuyanagi, S. Saito, and K. Semba, Superconducting qubit-oscillator circuit beyond the ultrastrong-coupling regime, *Nature Physics* **13**, 44 (2017).
- [4] A. Bayer, M. Pozimski, S. Schambeck, D. Schuh, R. Huber, D. Bougeard, and C. Lange, Terahertz light-matter interaction beyond unity coupling strength, *Nano letters* **17**, 6340 (2017).
- [5] J. F. Poyatos, J. I. Cirac, and P. Zoller, Quantum reservoir engineering with laser cooled trapped ions, *Phys. Rev. Lett.* **77**, 4728 (1996).

- [6] M. B. Plenio and S. F. Huelga, Entangled light from white noise, *Phys. Rev. Lett.* **88**, 197901 (2002).
- [7] B. Kraus, H. P. Büchler, S. Diehl, A. Kantian, A. Micheli, and P. Zoller, Preparation of entangled states by quantum markov processes, *Phys. Rev. A* **78**, 042307 (2008).
- [8] Z. Leghtas, S. Touzard, I. M. Pop, A. Kou, B. Vlastakis, A. Petrenko, K. M. Sliwa, A. Narla, S. Shankar, M. J. Hatridge, *et al.*, Confining the state of light to a quantum manifold by engineered two-photon loss, *Science* **347**, 853 (2015).
- [9] E. M. Kessler, G. Giedke, A. Imamoglu, S. F. Yelin, M. D. Lukin, and J. I. Cirac, Dissipative phase transition in a central spin system, *Phys. Rev. A* **86**, 012116 (2012).
- [10] H. J. Carmichael, Breakdown of photon blockade: A dissipative quantum phase transition in zero dimensions, *Phys. Rev. X* **5**, 031028 (2015).
- [11] R. Puebla, M.-J. Hwang, J. Casanova, and M. B. Plenio, Probing the dynamics of a superradiant quantum phase transition with a single trapped ion, *Phys. Rev. Lett.* **118**, 073001 (2017).
- [12] F. Minganti, A. Biella, N. Bartolo, and C. Ciuti, Spectral theory of liouvillians for dissipative phase transitions, *Phys. Rev. A* **98**, 042118 (2018).
- [13] J. B. Curtis, I. Boettcher, J. T. Young, M. F. Maghrebi, H. Carmichael, A. V. Gorshkov, and M. Foss-Feig, Critical theory for the breakdown of photon blockade, *Phys. Rev. Res.* **3**, 023062 (2021).
- [14] S. R. K. Rodriguez, W. Casteels, F. Storme, N. Carlon Zambon, I. Sagnes, L. Le Gratiet, E. Galopin, A. Lemaître, A. Amo, C. Ciuti, and J. Bloch, Probing a dissipative phase transition via dynamical optical hysteresis, *Phys. Rev. Lett.* **118**, 247402 (2017).
- [15] T. Fink, A. Schade, S. Höfling, C. Schneider, and A. Imamoglu, Signatures of a dissipative phase transition in photon correlation measurements, *Nature Physics* **14**, 365 (2018).
- [16] G. Beaulieu, F. Minganti, S. Frasca, V. Savona, S. Felicetti, R. Di Candia, and P. Scarlino, Observation of first-and second-order dissipative phase transitions in a two-photon driven kerr resonator, *Nature communications* **16**, 1954 (2025).
- [17] J. Raftery, D. Sadri, S. Schmidt, H. E. Türeci, and A. A. Houck, Observation of a dissipation-induced classical to quantum transition, *Phys. Rev. X* **4**, 031043 (2014).
- [18] M. Fitzpatrick, N. M. Sundaresan, A. C. Y. Li, J. Koch, and A. A. Houck, Observation of a dissipative phase transition in a one-dimensional circuit qed lattice, *Phys. Rev. X* **7**, 011016 (2017).
- [19] P. Brookes, G. Tancredi, A. D. Patterson, J. Rahamim, M. Esposito, T. K. Mavrogordatos, P. J. Leek, E. Giannossar, and M. H. Szymanska, Critical slowing down in circuit quantum electrodynamics, *Science advances* **7**, eabe9492 (2021).
- [20] F. Bibak, U. c. v. Delić, M. Aspelmeyer, and B. Dakić, Dissipative phase transitions in optomechanical systems, *Phys. Rev. A* **107**, 053505 (2023).
- [21] J. M. Lee, H.-W. Lee, and M.-J. Hwang, Cavity magnonics with easy-axis ferromagnets: Critically enhanced magnon squeezing and light-matter interaction, *Phys. Rev. B* **108**, L241404 (2023).
- [22] B. Wang, F. Nori, and Z.-L. Xiang, Quantum phase transitions in optomechanical systems, *Phys. Rev. Lett.* **132**, 053601 (2024).
- [23] J. M. Lee, H.-W. Lee, and M.-J. Hwang, Diverging en-

tanglement of critical magnons in easy-axis antiferromagnets, *Phys. Rev. B* **111**, 094402 (2025).

[24] M.-J. Hwang, P. Rabl, and M. B. Plenio, Dissipative phase transition in the open quantum Rabi model, *Phys. Rev. A* **97**, 013825 (2018).

[25] M.-L. Cai, Z.-D. Liu, Y. Jiang, Y.-K. Wu, Q.-X. Mei, W.-D. Zhao, L. He, X. Zhang, Z.-C. Zhou, and L.-M. Duan, Probing a dissipative phase transition with a trapped ion through reservoir engineering, *Chinese Physics Letters* **39**, 020502 (2022).

[26] P. Sierant, G. Chiriacò, F. M. Surace, S. Sharma, X. Turkeshi, M. Dalmonte, R. Fazio, and G. Pagano, Dissipative floquet dynamics: From steady state to measurement induced criticality in trapped-ion chains, *Quantum* **6**, 638 (2022).

[27] K. Baumann, C. Guerlin, F. Brennecke, and T. Esslinger, Dicke quantum phase transition with a superfluid gas in an optical cavity, *Nature* **464**, 1301 (2010).

[28] F. Brennecke, R. Mottl, K. Baumann, R. Landig, T. Donner, and T. Esslinger, Real-time observation of fluctuations at the driven-dissipative Dicke phase transition, *Proceedings of the National Academy of Sciences* **110**, 11763 (2013).

[29] J. Klinder, H. Keßler, M. Wolke, L. Mathey, and A. Hemmerich, Dynamical phase transition in the open Dicke model, *Proceedings of the National Academy of Sciences* **112**, 3290 (2015).

[30] G. Lyu, K. Kottmann, M. B. Plenio, and M.-J. Hwang, Multicritical dissipative phase transitions in the anisotropic open quantum Rabi model, *Phys. Rev. Res.* **6**, 033075 (2024).

[31] B. Buća and T. Prosen, A note on symmetry reductions of the lindblad equation: transport in constrained open spin chains, *New Journal of Physics* **14**, 073007 (2012).

[32] V. V. Albert and L. Jiang, Symmetries and conserved quantities in lindblad master equations, *Phys. Rev. A* **89**, 022118 (2014).

[33] J. Y. Lee, C.-M. Jian, and C. Xu, Quantum criticality under decoherence or weak measurement, *PRX Quantum* **4**, 030317 (2023).

[34] P. Sala, S. Gopalakrishnan, M. Oshikawa, and Y. You, Spontaneous strong symmetry breaking in open systems: Purification perspective, *Phys. Rev. B* **110**, 155150 (2024).

[35] L. A. Lessa, R. Ma, J.-H. Zhang, Z. Bi, M. Cheng, and C. Wang, Strong-to-weak spontaneous symmetry breaking in mixed quantum states, *PRX Quantum* **6**, 010344 (2025).

[36] Z. Liu, L. Chen, Y. Zhang, S. Zhou, and P. Zhang, Diagnosing strong-to-weak symmetry breaking via wightman correlators, *Communications Physics* **8**, 274 (2025).

[37] N. Ziereis, S. Moudgalya, and M. Knap, Strong-to-weak symmetry breaking phases in steady states of quantum operations (2025), arXiv:2509.09669 [cond-mat.stat-mech].

[38] D. Gu, Z. Wang, and Z. Wang, Spontaneous symmetry breaking in open quantum systems: Strong, weak, and strong-to-weak, *Phys. Rev. B* **112**, 245123 (2025).

[39] C. Zhang, Y. Xu, J.-H. Zhang, C. Xu, Z. Bi, and Z.-X. Luo, Strong-to-weak spontaneous breaking of 1-form symmetry and intrinsically mixed topological order, *Phys. Rev. B* **111**, 115137 (2025).

[40] Y. Guo and S. Yang, Strong-to-weak spontaneous symmetry breaking meets average symmetry-protected topological order, *Phys. Rev. B* **111**, L201108 (2025).

[41] X. Huang, M. Qi, J.-H. Zhang, and A. Lucas, Hydrodynamics as the effective field theory of strong-to-weak spontaneous symmetry breaking, *Phys. Rev. B* **111**, 125147 (2025).

[42] S. Lieu, R. Belyansky, J. T. Young, R. Lundgren, V. V. Albert, and A. V. Gorshkov, Symmetry breaking and error correction in open quantum systems, *Phys. Rev. Lett.* **125**, 240405 (2020).

[43] Y.-J. Liu and S. Lieu, Dissipative phase transitions and passive error correction, *Phys. Rev. A* **109**, 022422 (2024).

[44] Y. Zhu and M.-J. Hwang, Passive error correction with a qubit-oscillator system in noisy environment, *Journal of the Korean Physical Society* **85**, 890 (2024).

[45] N. Sun, P. Zhang, and L. Feng, Scheme to detect the strong-to-weak symmetry breaking via randomized measurements, *Phys. Rev. Lett.* **135**, 090403 (2025).

[46] X. Feng, Z. Cheng, and M. Ippoliti, Hardness of observing strong-to-weak symmetry breaking, *Phys. Rev. Lett.* **135**, 200402 (2025).

[47] L. M. Sieberer, S. D. Huber, E. Altman, and S. Diehl, Dynamical critical phenomena in driven-dissipative systems, *Phys. Rev. Lett.* **110**, 195301 (2013).

[48] A. Altland, M. Fleischhauer, and S. Diehl, Symmetry classes of open fermionic quantum matter, *Phys. Rev. X* **11**, 021037 (2021).

[49] L. Sá, P. Ribeiro, and T. c. v. Prosen, Symmetry classification of many-body lindbladians: Tenfold way and beyond, *Phys. Rev. X* **13**, 031019 (2023).

[50] L. M. Sieberer, M. Buchhold, J. Marino, and S. Diehl, Universality in driven open quantum matter, *Rev. Mod. Phys.* **97**, 025004 (2025).

[51] M.-J. Hwang, R. Puebla, and M. B. Plenio, Quantum phase transition and universal dynamics in the Rabi model, *Phys. Rev. Lett.* **115**, 180404 (2015).

[52] P. Kirton, M. M. Roses, J. Keeling, and E. G. Dalla Torre, Introduction to the Dicke model: From equilibrium to nonequilibrium, and vice versa, *Advanced Quantum Technologies* **2**, 1800043 (2019).

[53] M. Mirrahimi, Z. Leghtas, V. V. Albert, S. Touzard, R. J. Schoelkopf, L. Jiang, and M. H. Devoret, Dynamically protected cat-qubits: a new paradigm for universal quantum computation, *New Journal of Physics* **16**, 045014 (2014).

[54] N. Bartolo, F. Minganti, W. Casteels, and C. Ciuti, Exact steady state of a kerr resonator with one- and two-photon driving and dissipation: Controllable wigner-function multimodality and dissipative phase transitions, *Phys. Rev. A* **94**, 033841 (2016).

[55] D. Roberts and A. A. Clerk, Driven-dissipative quantum kerr resonators: New exact solutions, photon blockade and quantum bistability, *Phys. Rev. X* **10**, 021022 (2020).

[56] V. Y. Mylnikov, S. O. Potashin, G. S. Sokolovskii, and N. S. Averkiev, Emergent equilibrium and quantum criticality in a two-photon dissipative oscillator, *Phys. Rev. Res.* **7**, 013061 (2025).

[57] E. G. Dalla Torre, E. Demler, T. Giamarchi, and E. Altman, Dynamics and universality in noise-driven dissipative systems, *Phys. Rev. B* **85**, 184302 (2012).

[58] S. Mathey and S. Diehl, Absence of criticality in the phase transitions of open floquet systems, *Phys. Rev. Lett.* **122**, 110602 (2019).

[59] M. Kang, Y. Zhang, K. R. Brown, and T. Barthel,

Non-gaussian phase transition and cascade of instabilities in the dissipative quantum Rabi model (2025), arXiv:2507.07092 [quant-ph].

[60] E. G. D. Torre, S. Diehl, M. D. Lukin, S. Sachdev, and P. Strack, Keldysh approach for nonequilibrium phase transitions in quantum optics: Beyond the Dicke model in optical cavities, *Phys. Rev. A* **87**, 023831 (2013).

[61] L. M. Sieberer, M. Buchhold, and S. Diehl, Keldysh field theory for driven open quantum systems, *Reports on Progress in Physics* **79**, 096001 (2016).

[62] A. Mari and J. Eisert, Cooling by heating: Very hot thermal light can significantly cool quantum systems, *Physical review letters* **108**, 120602 (2012).

[63] M. Woolley and A. Clerk, Two-mode squeezed states in cavity optomechanics via engineering of a single reservoir, *Physical Review A* **89**, 063805 (2014).

[64] R. Kubo, Generalized cumulant expansion method, *Journal of the Physical Society of Japan* **17**, 1100 (1962).

[65] F. Reiter, T. L. Nguyen, J. P. Home, and S. F. Yelin, Cooperative breakdown of the oscillator blockade in the dicke model, *Phys. Rev. Lett.* **125**, 233602 (2020).

[66] P. Fowler-Wright, K. B. Arnardóttir, P. Kirton, B. W. Lovett, and J. Keeling, Determining the validity of cumulant expansions for central spin models, *Phys. Rev. Res.* **5**, 033148 (2023).

[67] A. A. Clerk, M. H. Devoret, S. M. Girvin, F. Marquardt, and R. J. Schoelkopf, Introduction to quantum noise, measurement, and amplification, *Rev. Mod. Phys.* **82**, 1155 (2010).

[68] A. Blais, A. L. Grimsmo, S. M. Girvin, and A. Wallraff, Circuit quantum electrodynamics, *Rev. Mod. Phys.* **93**, 025005 (2021).

[69] P. Zanardi and M. Rasetti, Noiseless quantum codes, *Phys. Rev. Lett.* **79**, 3306 (1997).

[70] D. A. Lidar, I. L. Chuang, and K. B. Whaley, Decoherence-free subspaces for quantum computation, *Phys. Rev. Lett.* **81**, 2594 (1998).

[71] A. Jayesh Shah, P. Kirton, S. Felicetti, and H. Alaeian, Dissipative phase transition in the two-photon Dicke model, *Phys. Rev. Lett.* **135**, 173602 (2025).

[72] A. I. Lvovsky and M. G. Raymer, Continuous-variable optical quantum-state tomography, *Rev. Mod. Phys.* **81**, 299 (2009).

[73] C. Sánchez Muñoz, B. Buća, J. Tindall, A. González-Tudela, D. Jaksch, and D. Porras, Symmetries and conservation laws in quantum trajectories: Dissipative freezing, *Phys. Rev. A* **100**, 042113 (2019).

[74] J. Tindall, D. Jaksch, and C. S. Muñoz, On the generality of symmetry breaking and dissipative freezing in quantum trajectories, *SciPost Phys. Core* **6**, 004 (2023).

[75] M. E. Fisher and M. N. Barber, Scaling theory for finite-size effects in the critical region, *Phys. Rev. Lett.* **28**, 1516 (1972).

[76] R. Botet, R. Jullien, and P. Pfeuty, Size scaling for infinitely coordinated systems, *Phys. Rev. Lett.* **49**, 478 (1982).

[77] P. C. Hohenberg and B. I. Halperin, Theory of dynamic critical phenomena, *Rev. Mod. Phys.* **49**, 435 (1977).

[78] See supplemental material for further details that include Refs. [65, 66].

[79] A. Serafini, *Quantum continuous variables: a primer of theoretical methods* (CRC press, 2023).

## End Matter

*Langevin equation approach.*—As an alternative to the Keldysh calculation of the Gaussian fluctuations, we analyze here the Gaussian quantum fluctuations around the steady state by linearizing the Langevin equations and solving the corresponding Lyapunov equation for the steady-state covariance matrix.

We consider fluctuations  $\delta a = a - \langle a \rangle$  around the mean-field solution and introduce the quadrature fluctuation operators

$$X = \frac{\delta a + \delta a^\dagger}{\sqrt{2}}, \quad P = \frac{\delta a - \delta a^\dagger}{i\sqrt{2}}. \quad (14)$$

Starting from the Lindblad master equation [Eq. (1)], the linearized Langevin equation for the quadrature fluctuations takes the form

$$\dot{\mathbf{R}} = A\mathbf{R} + \boldsymbol{\eta}, \quad \langle \boldsymbol{\eta}(t)\boldsymbol{\eta}^T(t') \rangle = D\delta(t - t'), \quad (15)$$

where  $\mathbf{R} = (X, P)^T$ . The drift matrix  $A$  is obtained by linearizing both the coherent Hamiltonian dynamics and the nonlinear dissipative terms. We have

$$A = \begin{pmatrix} 6\rho & \omega - 2\lambda \\ -\omega - 2\lambda & 2\rho \end{pmatrix}, \quad (16)$$

with  $\rho = \kappa_2|\langle a \rangle|^2$ . In the superradiant phase, the two-photon loss generates quadrature-dependent effective damping once the condensate amplitude  $\langle a \rangle$  becomes finite. The noise vector  $\boldsymbol{\eta} = (\eta_X, \eta_P)^T$  is defined as

$$\eta_X = \frac{a_{\text{in}} + a_{\text{in}}^\dagger}{\sqrt{2}}, \quad \eta_P = \frac{a_{\text{in}} - a_{\text{in}}^\dagger}{i\sqrt{2}}, \quad (17)$$

where

$$a_{\text{in}} = \sqrt{\kappa_1}a_{1,\text{in}} + 2\sqrt{\rho}a_{2,\text{in}}, \quad (18)$$

and the input noise operators satisfy  $\langle a_{i,\text{in}}(t)a_{j,\text{in}}^\dagger(t') \rangle = \delta_{ij}\delta(t - t')$ . The noise correlations follow from the linearized dissipator and correspond to vacuum input noise associated with single- and two-photon loss channels. The corresponding diffusion matrix is isotropic,  $D = \Gamma\mathcal{I}_2$ , where  $\Gamma = \kappa_1 + 4\rho$ . This Langevin description fully captures the Gaussian fluctuations around the mean-field solution.

We now compute the static Gaussian fluctuations. The covariance matrix of the quadratures is defined as

$$V = \begin{pmatrix} \langle X^2 \rangle & \frac{1}{2}\langle XP + PX \rangle \\ \frac{1}{2}\langle XP + PX \rangle & \langle P^2 \rangle \end{pmatrix}. \quad (19)$$

For a Gaussian bosonic system,  $V$  satisfies the Lyapunov equation [62, 63].

$$AV + VA^T + D = 0. \quad (20)$$

Solving Eq. (20), we obtain closed forms

$$\begin{aligned} \langle X^2 \rangle &= \frac{c_3(\Omega_1^2 + \Omega_1\Omega_2 + c_1c_2 + c_2^2)}{2(c_1 + c_2)(\Omega_1\Omega_2 + c_1c_2)}, \\ \langle P^2 \rangle &= \frac{c_3(\Omega_1\Omega_2 + \Omega_2^2 + c_1^2 + c_1c_2)}{2(c_1 + c_2)(\Omega_1\Omega_2 + c_1c_2)}, \\ \frac{1}{2}\langle XP + PX \rangle &= \frac{c_3(\Omega_1c_1 - \Omega_2c_2)}{2(c_1 + c_2)(\Omega_1\Omega_2 + c_1c_2)}, \end{aligned} \quad (21)$$

where  $\Omega_1 = \omega - 2\lambda$ ,  $\Omega_2 = \omega + 2\lambda$ ,  $c_1 = 6\rho + \kappa_1$ ,  $c_2 = 2\rho + \kappa_1$ , and  $c_3 = 4\rho + \kappa_1$ . The number and squeezing fluctuations are related to the covariance matrix elements as

$$\begin{aligned} \delta n &= \frac{1}{2}(\langle X^2 \rangle + \langle P^2 \rangle - 1), \\ \text{Re}[\delta m] &= \frac{1}{2}(\langle X^2 \rangle - \langle P^2 \rangle), \\ \text{Im}[\delta m] &= \frac{1}{2}\langle XP + PX \rangle. \end{aligned} \quad (22)$$

For a Gaussian bosonic state, the purity is given by [79]

$$\mu = \frac{1}{\sqrt{4\langle X^2 \rangle \langle P^2 \rangle - \langle XP + PX \rangle^2}}. \quad (23)$$

Expanding these expressions near the critical point  $\lambda = \lambda_c$ , we find results identical to those obtained from the Keldysh path-integral approach in the main text, as summarized in Table I.

*One-loop calculation.*—We present the one-loop correction arising from the quartic interaction generated by the two-photon loss within the Keldysh path-integral formalism [61].

The quartic contribution to the Keldysh action originating from the two-photon loss reads

$$S^{(4)} = i\kappa_2 \int dt \mathcal{V}(t), \quad (24)$$

with

$$\mathcal{V}(t) = a_c^* a_q^* (a_c^2 + a_q^2) - (a_c^{*2} + a_q^{*2}) a_c a_q + 4a_c^* a_c a_q^* a_q. \quad (25)$$

The Green function in the presence of the quartic interaction,  $G^{\alpha\beta}(t_1, t_2) = \langle \psi_\alpha(t_1) \psi_\beta^*(t_2) \rangle$ , admits the perturbative expansion

$$\begin{aligned} G^{\alpha\beta}(t_1, t_2) &= G_0^{\alpha\beta}(t_1, t_2) + \langle \psi_\alpha(t_1) \psi_\beta^*(t_2) S^{(4)} \rangle_0 \\ &\quad - \frac{i}{2} \langle \psi_\alpha(t_1) \psi_\beta^*(t_2) (S^{(4)})^2 \rangle_0 + \dots, \end{aligned} \quad (26)$$

where  $\langle \dots \rangle_0$  denotes the Gaussian average defined by the quadratic Keldysh action. The last term is of order  $O(\kappa_2^2)$  and corresponds to a two-loop contribution. In the following, we focus on the leading one-loop correction,

$$\delta G^{\alpha\beta}(t_1, t_2) = i\kappa_2 \int dt \langle \psi_\alpha(t_1) \psi_\beta^*(t_2) \mathcal{V}(t) \rangle_0. \quad (27)$$

Using Wick's theorem and the temporal locality of  $S^{(4)}$ , the correction to the retarded Green function is given by

$$\delta G^R(t_1 - t_2) = \int dt G_0^R(t_1 - t) \Sigma^R G_0^R(t - t_2), \quad (28)$$

where  $\Sigma^R$  is the retarded self-energy matrix. The bare retarded Green function in the Nambu-Keldysh basis is

$$G_0^R(t) = -i \begin{pmatrix} \langle a_c(t) a_q^*(0) \rangle_0 & \langle a_c(t) a_q(0) \rangle_0 \\ \langle a_c^*(t) a_q^*(0) \rangle_0 & \langle a_c^*(t) a_q(0) \rangle_0 \end{pmatrix}. \quad (29)$$

The self-energy is determined by equal-time contractions involving one classical and one quantum field, which are obtained from the second functional derivatives of  $S^{(4)}$ ,

$$\begin{aligned} \frac{\delta^2 S^{(4)}}{\delta a_c \delta a_q^*} &= i\kappa_2 (2a_c^* a_c - 2a_q^* a_q + 4a_c^* a_q), \\ \frac{\delta^2 S^{(4)}}{\delta a_c^* \delta a_q} &= i\kappa_2 (-2a_c^* a_c + 2a_q^* a_q + 4a_q^* a_c), \\ \frac{\delta^2 S^{(4)}}{\delta a_c \delta a_q} &= i\kappa_2 (-a_c^{*2} - a_q^{*2} + 4a_c^* a_q^*), \\ \frac{\delta^2 S^{(4)}}{\delta a_c^* \delta a_q^*} &= i\kappa_2 (a_c^2 + a_q^2 + 4a_c a_q). \end{aligned} \quad (30)$$

Here, the one-loop contribution for the retarded Green function corresponds diagrammatically to the loop diagrams shown in Fig. 1(c) of the main text, which represent the quartic-order corrections generated by the two-photon loss.

From the Dyson equation

$$[G^R(\nu)]^{-1} = [G_0^R(\nu)]^{-1} - \Sigma^R, \quad (31)$$

we obtain the retarded Green function with the one-loop correction quoted in Eq. (11) of the main text. Similarly, the Keldysh self-energy acquires the correction

$$\Sigma^K = 2i(\Gamma + 2\kappa_2 n) \mathcal{I}_2, \quad (32)$$

which renormalizes the noise kernel. Using the corrected Keldysh action and the relations in Eq. (6), we determine the number and squeezing fluctuations by setting the critical point  $\lambda = \lambda_c$  [60]. Expanding the solutions for small  $\kappa_2$  yields the scaling behavior summarized in Table II of the main text.

# Supplemental Material for “Universality classes split by strong and weak symmetries”

Jongjun M. Lee\* and Igor Boettcher†

*Department of Physics, University of Alberta, Edmonton, Alberta T6G 2E1, Canada and  
Quantum Horizons Alberta & Theoretical Physics Institute,  
University of Alberta, Edmonton, Alberta T6G 2E1, Canada*

Myung-Joong Hwang‡

*Division of Natural and Applied Sciences, Duke Kunshan University, Kunshan, Jiangsu 215300, China*  
(Dated: February 11, 2026)

## CONTENTS

A. Detailed calculation of the cumulant expansion	1
B. Supplemental figures - numerical data from the cumulant expansion	2
References	2

### Appendix A: Detailed calculation of the cumulant expansion

We employ a cumulant expansion to incorporate higher-order correlations and to verify the non-Gaussian critical scaling behavior. We start from the Lindblad master equation introduced in the main text as follows.

$$\frac{\partial \rho}{\partial t} = \mathcal{L}[\rho] = -i[H, \rho] + \sum_{j=1,2} \mathcal{D}[L_j], \quad (\text{A1})$$

where

$$H = \omega a^\dagger a + \lambda(a^2 + a^{\dagger 2}), \quad (\text{A2})$$

$L_1 = \sqrt{\kappa_1}a$ ,  $L_2 = \sqrt{\kappa_2}a^2$ , and  $\mathcal{D}[L] = 2L\rho L^\dagger - L^\dagger L\rho - \rho L^\dagger L$ . From this, we derive the following equations of motion for the first and second moments.

$$\begin{aligned} \frac{d\langle a \rangle}{dt} &= - (i\omega + \kappa_1)\langle a \rangle - 2i\lambda\langle a \rangle^* - 2\kappa_2\langle a^\dagger a^2 \rangle, \\ \frac{dm}{dt} &= - 2(i\omega + \kappa_1 + \kappa_2)m - 2i\lambda - 4i\lambda n \\ &\quad - 4\kappa_2\langle a^\dagger a^3 \rangle, \\ \frac{dn}{dt} &= + 2i\lambda(m - m^*) - 2\kappa_1n - 4\kappa_2\langle a^{\dagger 2}a^2 \rangle. \end{aligned} \quad (\text{A3})$$

To close the hierarchy, we apply a cumulant expansion and truncate the connected correlators beyond second order, which provides a controlled approximation capturing leading non-Gaussian corrections near the critical point [1, 2]. The general formulae for three- and four-point correlators are given by

$$\langle \mathcal{O}_1 \mathcal{O}_2 \mathcal{O}_3 \rangle \simeq \langle \mathcal{O}_1 \mathcal{O}_2 \rangle \langle \mathcal{O}_3 \rangle + \langle \mathcal{O}_1 \mathcal{O}_3 \rangle \langle \mathcal{O}_2 \rangle + \langle \mathcal{O}_2 \mathcal{O}_3 \rangle \langle \mathcal{O}_1 \rangle - 2\langle \mathcal{O}_1 \rangle \langle \mathcal{O}_2 \rangle \langle \mathcal{O}_3 \rangle, \quad (\text{A4})$$

and

$$\begin{aligned} \langle \mathcal{O}_1 \mathcal{O}_2 \mathcal{O}_3 \mathcal{O}_4 \rangle &\simeq \langle \mathcal{O}_1 \mathcal{O}_2 \rangle \langle \mathcal{O}_3 \mathcal{O}_4 \rangle + \langle \mathcal{O}_1 \mathcal{O}_3 \rangle \langle \mathcal{O}_2 \mathcal{O}_4 \rangle + \langle \mathcal{O}_1 \mathcal{O}_4 \rangle \langle \mathcal{O}_2 \mathcal{O}_3 \rangle + \langle \mathcal{O}_1 \rangle \langle \mathcal{O}_2 \mathcal{O}_3 \mathcal{O}_4 \rangle + \langle \mathcal{O}_2 \rangle \langle \mathcal{O}_1 \mathcal{O}_3 \mathcal{O}_4 \rangle \\ &\quad + \langle \mathcal{O}_1 \mathcal{O}_2 \mathcal{O}_4 \rangle \langle \mathcal{O}_3 \rangle + \langle \mathcal{O}_1 \mathcal{O}_2 \mathcal{O}_3 \rangle \langle \mathcal{O}_4 \rangle - 2\langle \mathcal{O}_1 \rangle \langle \mathcal{O}_2 \rangle \langle \mathcal{O}_3 \mathcal{O}_4 \rangle - 2\langle \mathcal{O}_1 \rangle \langle \mathcal{O}_2 \mathcal{O}_3 \rangle \langle \mathcal{O}_4 \rangle \\ &\quad - 2\langle \mathcal{O}_1 \rangle \langle \mathcal{O}_2 \mathcal{O}_4 \rangle \langle \mathcal{O}_3 \rangle - 2\langle \mathcal{O}_1 \mathcal{O}_2 \rangle \langle \mathcal{O}_3 \rangle \langle \mathcal{O}_4 \rangle - 2\langle \mathcal{O}_1 \mathcal{O}_3 \rangle \langle \mathcal{O}_2 \rangle \langle \mathcal{O}_4 \rangle - 2\langle \mathcal{O}_1 \mathcal{O}_4 \rangle \langle \mathcal{O}_2 \rangle \langle \mathcal{O}_3 \rangle \\ &\quad + 6\langle \mathcal{O}_1 \rangle \langle \mathcal{O}_2 \rangle \langle \mathcal{O}_3 \rangle \langle \mathcal{O}_4 \rangle, \end{aligned} \quad (\text{A5})$$

\* Contact author: jongjun@ualberta.ca

† Contact author: iboettch@ualberta.ca

‡ Contact author: myungjoong.hwang@duke.edu

where  $\mathcal{O}_{j=1,2,3,4}$  is the arbitrary operator. Applying these relations, the higher-order correlators appearing in the above equations of motion reduce to

$$\begin{aligned}\langle a^\dagger a^2 \rangle &\simeq +2n\langle a \rangle + m\langle a \rangle^* - 2\langle a \rangle |\langle a \rangle|^2, \\ \langle a^\dagger a^3 \rangle &\simeq -2\langle a \rangle |\langle a \rangle|^2 + 3nm, \\ \langle a^\dagger a^2 \rangle &\simeq +|m|^2 + 2n^2 - 2|\langle a \rangle|^4.\end{aligned}\quad (\text{A6})$$

Assuming a steady state, we obtain a closed set of coupled equations for the three variables  $\langle a \rangle$ ,  $n$ , and  $m$ .

$$\begin{aligned}0 &= -(i\omega + \kappa_1)\langle a \rangle - 2i\lambda\langle a \rangle^* - 2\kappa_2(+2n\langle a \rangle + m\langle a \rangle^* - 2\langle a \rangle |\langle a \rangle|^2), \\ 0 &= -2(i\omega + \kappa_1 + \kappa_2)m - 2i\lambda - 4i\lambda n - 4\kappa_2(-2\langle a \rangle |\langle a \rangle|^2 + 3nm), \\ 0 &= +2i\lambda(m - m^*) - 2\kappa_1 n - 4\kappa_2(|m|^2 + 2n^2 - 2|\langle a \rangle|^4).\end{aligned}\quad (\text{A7})$$

Note that these equations explicitly depend on the effective scaling parameter  $\kappa_2$ , and therefore the resulting solutions capture corrections beyond the Gaussian limit. By numerically solving these equations, we obtain the results shown in the main text and the Supplemental Material.

We note that for any finite  $\kappa_2$ , the exact steady state of the full Lindblad dynamics preserves parity symmetry and therefore satisfies  $\langle a \rangle = 0$ . Accordingly, the nonzero solutions for  $\langle a \rangle$  obtained from the second-order cumulant equations are not steady states for finite  $\kappa_2$ , but rather should be understood as metastable states and their fluctuation around them. Crucially, such metastable solutions become asymptotically stable in the thermodynamic limit  $\kappa_2 \rightarrow 0$ , where their lifetime diverges.

## Appendix B: Supplemental figures - numerical data from the cumulant expansion

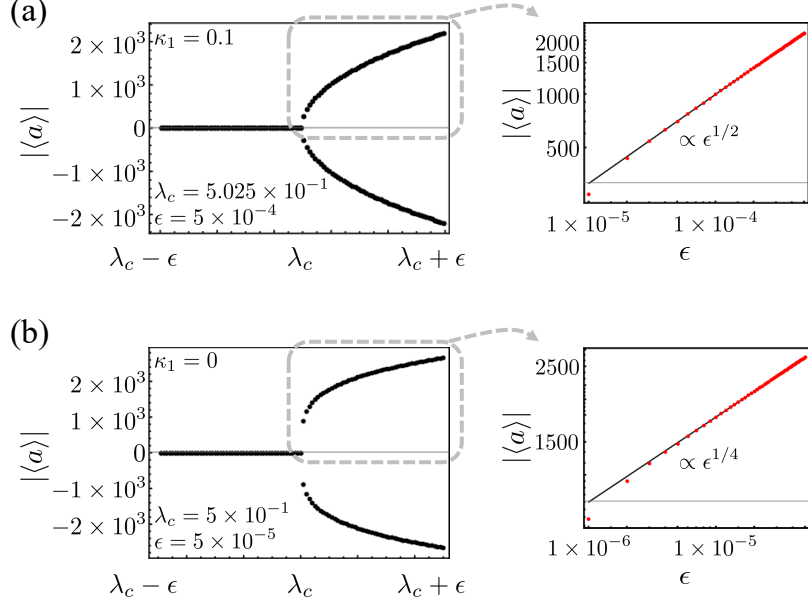


FIG. 1. Numerical results for the order-parameter amplitude  $|\langle a \rangle|$  as a function of the two-photon driving strength  $\lambda$ , obtained from the cumulant expansion. Panels (a) and (b) correspond to systems with weak parity symmetry and strong parity symmetry, respectively. The right panels show log-log plots of the superradiant phase, highlighting the scaling behavior.  $\epsilon$  denotes the deviation from the critical driving strength  $\lambda_c$ . The parameters are set to  $\omega = 1.0$  and  $\kappa_2 = 10^{-9}$  for all panels.

[1] P. Fowler-Wright, K. B. Arnardóttir, P. Kirton, B. W. Lovett, and J. Keeling, Determining the validity of cumulant expansions for central spin models, *Phys. Rev. Res.* **5**, 033148 (2023).

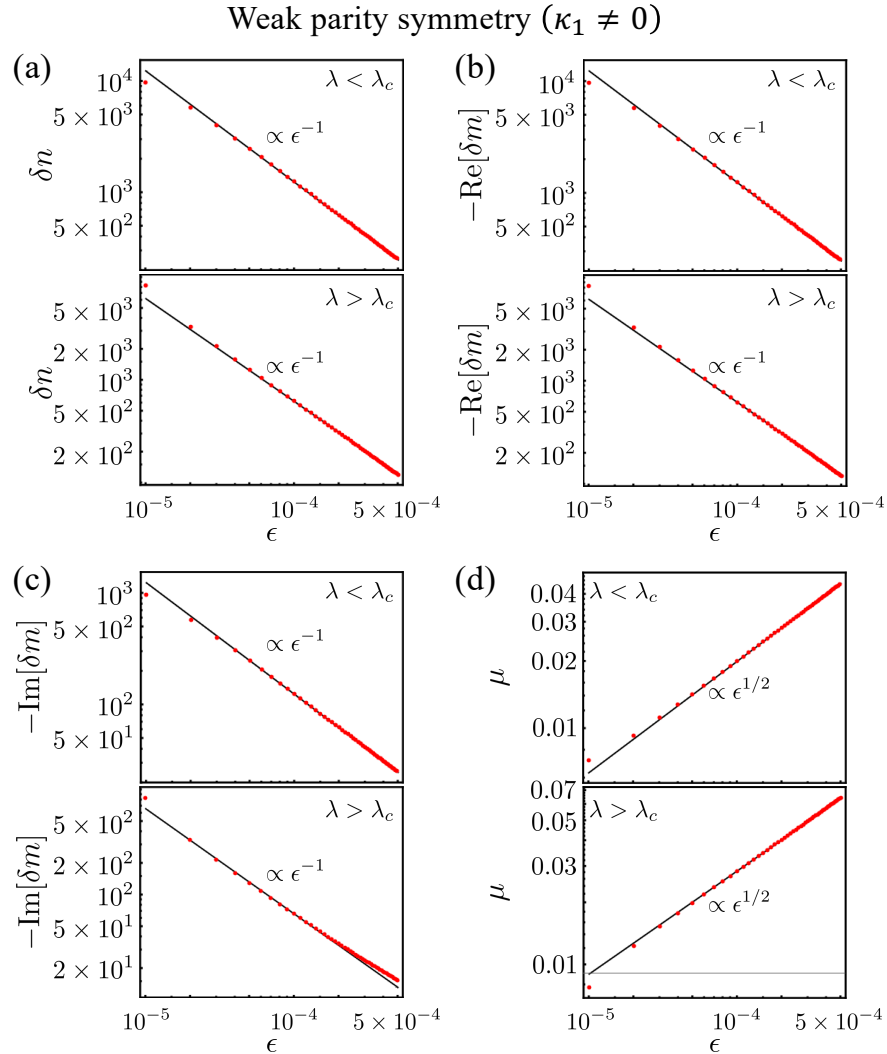


FIG. 2. Numerical results for the number fluctuation (a)  $\delta n$ , the squeezing fluctuations (b)  $\text{Re}[\delta m]$  and (c)  $\text{Im}[\delta m]$ , and the purity (d)  $\mu$  as functions of the two-photon driving strength  $\lambda$ , obtained from the cumulant expansion for a system with weak parity symmetry ( $\kappa_1 \neq 0$ ). Here,  $\epsilon$  denotes the deviation from the critical driving strength  $\lambda_c$ . All panels are shown on log-log scales, revealing the critical scaling behavior in the vicinity of the critical point. The parameters are set to  $\omega = 1.0$ ,  $\kappa_2 = 10^{-9}$ ,  $\kappa_1 = 0.1$ , and  $\lambda_c = 0.502494$  for all panels.

[2] F. Reiter, T. L. Nguyen, J. P. Home, and S. F. Yelin, Cooperative breakdown of the oscillator blockade in the dicke model, *Phys. Rev. Lett.* **125**, 233602 (2020).

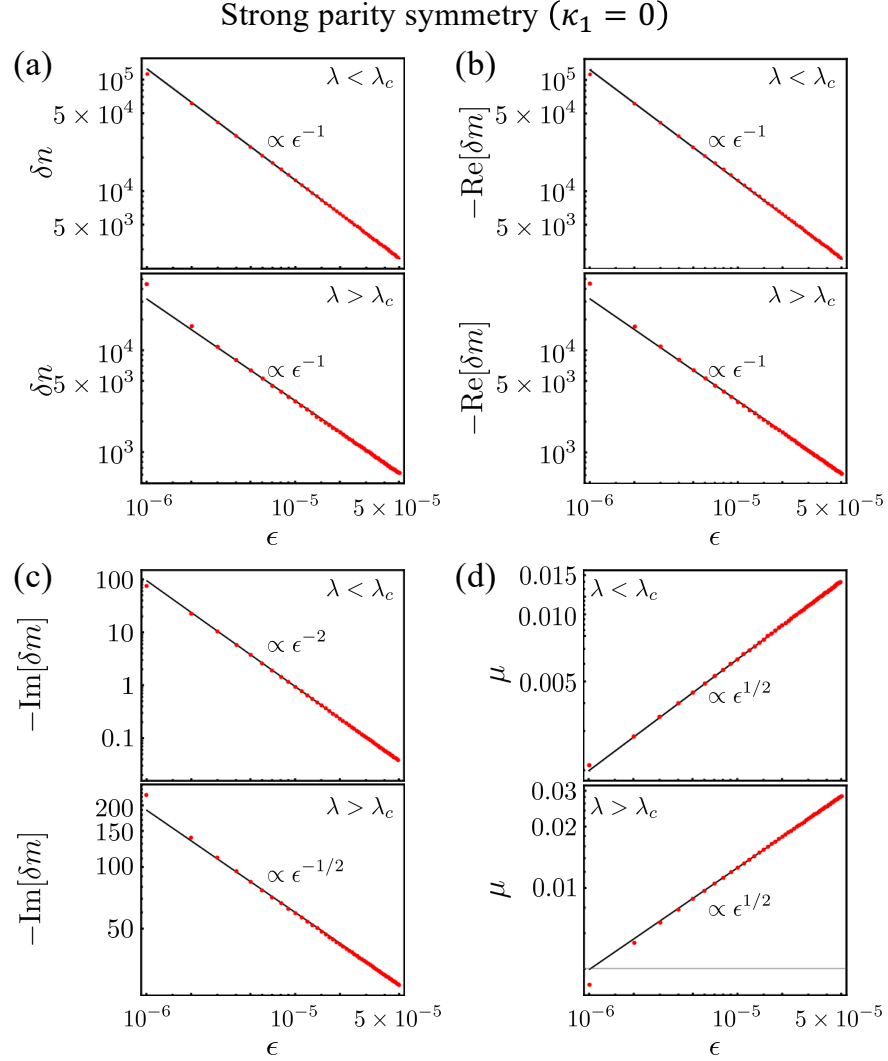


FIG. 3. Numerical results for the number fluctuation (a)  $\delta n$ , the squeezing fluctuations (b)  $\text{Re}[\delta m]$  and (c)  $\text{Im}[\delta m]$ , and the purity (d)  $\mu$  as functions of the two-photon driving strength  $\lambda$ , obtained from the cumulant expansion for a system with strong parity symmetry ( $\kappa_1 = 0$ ). Here,  $\epsilon$  denotes the deviation from the critical driving strength  $\lambda_c$ . All panels are shown on log-log scales, revealing the critical scaling behavior in the vicinity of the critical point. The parameters are set to  $\omega = 1.0$ ,  $\kappa_2 = 10^{-9}$ , and  $\lambda_c = 0.5$  for all panels.